

# **Analyzing the Role of Ripples in Information Integration in Mice**

Cognitive Science Honors Thesis

Yiting Bu

**Abstract**

The neural mechanisms underlying cortical integration remain incompletely understood. Recent human studies identified cortical ripples, bursts of high-frequency oscillations, as key events that synchronized activity across cortical areas via near-zero phase-lag co-occurrence (“co-ripples”), suggesting a mechanism for integration. In this study, we investigate cortical ripples in mice to characterize their properties, inter-area interactions, and modulation by tasks, aiming to extend our understanding of ripple mechanisms beyond what is accessible in human studies. By analyzing an open-source Neuropixels dataset from mouse visual cortex using current source density (CSD) methods, we demonstrate that cortical ripples and their co-occurrences across areas (co-ripples) are selectively modulated by task demands, cortical hierarchy, and cortical layers. Specifically, co-ripples occur most prominently during correct responses (hits), suggesting their direct role in perceptual decision-making. Overall, these findings validate mouse cortical ripples as a suitable model to study ripple-mediated integration observed in humans and highlight their synchronizing role during tasks. Ongoing analyses of ripple propagation and neuron-type specificity will further illuminate the fundamental process of cortical integration.

## Introduction

How does the brain integrate information from various sensory modalities to form a unified perception? Cortical integration, the process of combining distributed information, is central to conscious perception and serves as the foundation for higher-level cognition. Over the past decades, researchers have conducted extensive studies to understand the neural mechanisms underlying cortical integration, resulting in multiple theories (von der Malsburg et al. 1994; Singer et al., 1994; Revonsuo et al., 1999), yet so far, no consensus has been reached. One theory receiving much attention is the “binding-by-synchrony” hypothesis (BBS), which proposes that the cortex is bound through the temporal synchronization of neural activities (von der Malsburg et al., 1986; Fries et al., 2009). This theory has been met with both support and skepticism, backed by diverging experimental evidence (Shadlen et al., 1999; Gray et al., 1989; Singer, 2021; Vinck et al., 2023). In recent years, a growing body of research has turned its attention to ripples, stereotyped high-frequency neural oscillations, which seem to act as an essential substrate for synchronizing neuronal activity across the cortex, potentially underpinning BBS.

Initially identified in the hippocampus, ripples were shown to play a key role in memory consolidation, particularly during sharp-wave ripples (SWRs) observed in non-REM and offline states (Buzsaki et al., 2015). More recent studies have identified cortical ripples in humans, characterized by  $\sim 90$  Hz oscillation frequency and  $\sim 1000$  ms duration during both waking and non-REM sleep (Dickey et al., 2022). These cortical ripples have been found to synchronize activity across regions through co-occurrence (co-ripples) (Dickey et al., 2022), specifically through the means of coordinating and facilitating neuronal firings, which has been proved across a patch of the human cortex (Verzhbinsky et al., 2023). Further evidence points to their role in assisting integration across multiple cortical regions in humans during a cognitive task (Garrett et al., 2024).

While the existing studies in humans have highlighted the synchronizing role of cortical ripples, many mechanistic details remain unclear, partly due to the technical limitations of human intracranial recordings. For example, while ripples have been demonstrated to facilitate neuron firings, it is unknown how different categories of excitatory neurons and interneurons behave differently during co-ripples. Similarly, the layer-specific dynamics of ripple propagation, especially in task-related contexts, need more characterization. Mouse models, with their higher spatiotemporal resolution and large-scale datasets, provide a valuable system to investigate these mechanisms. However, most rodent studies to date have focused on hippocampal sharp wave ripples (Suh et al., 2013; Liu et al., 2017; Pedrosa et al., 2022), leaving cortical ripples relatively unexplored.

In this study, we leverage an open-source Neuropixels dataset from the Allen Institute to investigate the mechanisms of cortical ripples in the mouse visual cortex. Using current source

density (CSD) analysis, we detect ripples across multiple visual areas and examine their modulation by stimulus, task, and cortical layer. Although ripple events are sparse, they display distinct temporal and spatial patterns across stimulus blocks, aligned with visual cortical hierarchies. Co-ripples spanning visual areas show strong task modulation, with the highest occurrence during hit trials, as was found in previous work in humans (Garrett et al., 2024). Our studies in mice go beyond the human studies by adding granularity at the level of cortical hierarchy and laminar structure. Together, our results support the idea that cortico-cortical co-ripples are selectively engaged by task and sensory context and may contribute to cortical integration.

## Methods

### Open data sources

This study uses the Visual Behavior Neuropixels dataset released by the Allen Institute (2022). It includes 153 in vivo recording sessions from 81 mice (WT, Vip-IRES-Cre, Sst-IRES-Cre). Each mouse was implanted with 5 or 6 Neuropixels probes targeting six visual cortical areas: primary visual cortex (VISp), anterolateral visual area (VISal), lateral visual area (VISl), rostrolateral visual area (VISrl), anteromedial visual area (VISam), and posteromedial visual area (VISpm), as well as the hippocampus and thalamus. Each probe contained up to 384 recording channels with a vertical pitch of 20  $\mu\text{m}$ , and LFPs were sampled at 1250 Hz. The LFP traces were low-pass filtered at 1000 Hz and spatially downsampled by recording every three out of four channels, yielding an effective spatial resolution of 40  $\mu\text{m}$  along the probe. Spike sorting was performed using Kilosort2 (<https://github.com/mouseland/kilosort2>, commit 2fba667, April 8, 2019), with spike times sampled at 30 kHz and high-pass filtered at 500 Hz (Allen Institute, 2019). Quality metrics for each unit include firing rate, presence ratio, amplitude cutoff, inter-spike interval (ISI) violations, signal-to-noise ratio, isolation distance, d-prime, and nearest-neighbor hit rate. Optotagging was used to identify genetically defined interneuron subtypes (Sst- and Vip-expressing).

### Task description

Each recording session lasted approximately 155 minutes and included several distinct stimulus blocks. The first block, about 60 minutes long, was an active behavior task in which a pre-trained mouse viewed repeated flashes of natural images. Each image was shown for 250 milliseconds, followed by a 500-millisecond gray screen. The mouse was required to lick a reward port within 750 milliseconds of an image change to receive water. After this block, the port was removed,

and the mouse passively viewed stimuli including Gabors, spontaneous (blank screen), and full-field flashes for about 25 minutes. This was followed by a 60-minute passive replay block using the same natural images from the active block, but without any behavioral requirement or reward. The session concluded with a 10-minute optotagging protocol to identify Sst- and Vip-expressing interneurons. Each mouse typically completed two sessions: one using a familiar image set from training and one using a novel set. Each set contained 8 natural images, with 2 images shared in both.

### **Session selection**

Only sessions that included recordings from all six visual cortical areas were selected. Preliminary analysis showed that novel sessions generally contained a higher number of cortical ripples and co-ripples compared to familiar sessions. Therefore, only the novel sessions were analyzed in the current study. A total of 65 sessions met the selection criteria and were included in the analysis. Familiar sessions will be incorporated in future work.

### **Current source density**

Current source density (CSD) is the second spatial derivative of the local field potential (LFP), a measure of the currents flowing across neuronal membranes, assuming that, at least locally, such currents are determined only by the cortical layer (Fabó et al., 2013). In contrast to referential recordings, CSD is reference-free and thus not susceptible to the ambiguities regarding local generation that references often impose. In contrast to potential gradient, CSD is more focal, and also has a consistent relation to the direction of the local transmembrane currents, which in the case of ripples results in their polarity having a consistent relation to the predominant firing of local neurons, as is described below. This consistency enables meaningful measurements of phase consistency and lag between locations, as well as enabling LFP-unit modulation phase to be compared across units which permits reconstructing the order of firing of different cell-types across cortical layers and visual areas.. The full advantage of using CSD will not be realized until future studies. The optimal formula for computing CSD depends on the size and arrangement of the sources and sinks underlying the phenomenon of interest relative to the electrode pitch, For ripples in this dataset, we found that CSD was estimated adequately with the following simple formula:

$$CSD_{current\ channel} = \frac{1}{2}LFP_{channel\ above} + \frac{1}{2}LFP_{channel\ below} - LFP_{current\ channel}$$

### **Ripple detection**

Ripple detection was performed using a previously described ripple detection method originally developed for the human hippocampus (Jiang et al., 2019), then adapted for the human cortex

(Dickey et al., 2022) and further adapted here for the mouse cortex since they have a center frequency of  $\sim 146 \pm 5$  Hz (Khodagholy et al., 2018) whereas human cortical ripples have a central frequency of  $\sim 90$  Hz (Dickey et al., 2022). Specifically, LFP data were band-passed between 120–200 Hz, the frequency range characterized as cortical ripples in mice, using a zero phase-lag 6-pole Butterworth filter. Candidate events were identified where the ripple-band amplitude z-score exceeded 2.5, lasted at least 15 ms ( $\approx$  three cycles), and any events separated by  $\leq 20$  ms were merged. Ripple centers were set at the maximum positive peak. The ripple-band signal was z-scored individually for each channel, using that channel's mean and standard deviation computed across the entire recording. All other detection parameters were held constant across all channels, sessions, and animals.

Ripple boundaries were refined by applying a 16 ms Gaussian smoothing kernel to the z-scored envelope. Onset and offset were marked where the smoothed envelope crossed below 0.75. Events were rejected if any of the following applied: high-pass (100–300 Hz) z-score  $> 7$ , raw LFP amplitude beyond preset limits, abrupt amplitude jumps, fewer than three clear oscillations, or signs of artifact or contamination. Detection was performed using an adapted MATLAB script. All detected ripples were statistically verified, and  $\sim 1000$  ripples were visually reviewed at several sweep speeds and band-passes to confirm parameter selection and that with rare exceptions, selected events could be recognized as ripples. Channels that failed quality control were excluded from further analysis.

### **Ripple and co-ripple density**

Co-ripples are defined as ripple events in two regions whose durations overlap by  $\geq 12.5$  ms ( $\approx$  two cycles of ripple oscillation). Co-ripple density is the number of co-ripple events occurring per trial, averaging across all trials and sessions. Ripple density is the average rate of ripple onsets per channel per second, also averaged across trials.

### **Cortical layers**

Cortical layers are estimated using the Allen Institute's Common Coordinate Framework (CCF) mouse brain atlas (Wang et al., 2020), a 10  $\mu\text{m}$ -resolution 3D reference, with each channel's CCF coordinates drawn from the dataset; channel-to-layer mapping was adapted from the `layer_mapping.py` script (Allen Institute for Brain Science, 2020).

### **Data analysis**

Following ripple detection in MATLAB, all subsequent analyses were conducted in Python. The Allen Software Development Kit (Allen SDK) was used to access and query the dataset. Custom Python scripts were developed to perform data processing and analysis, allowing scalability across sessions and subjects. Visualization was carried out using Matplotlib (Hunter, 2007).

Statistical analyses were performed using SciPy (Virtanen et al., 2020), Statsmodels (Seabold & Perktold, 2010), and Pingouin (Vallat, 2018).

## Preliminary Results

### 1. Overview of ripple characteristics

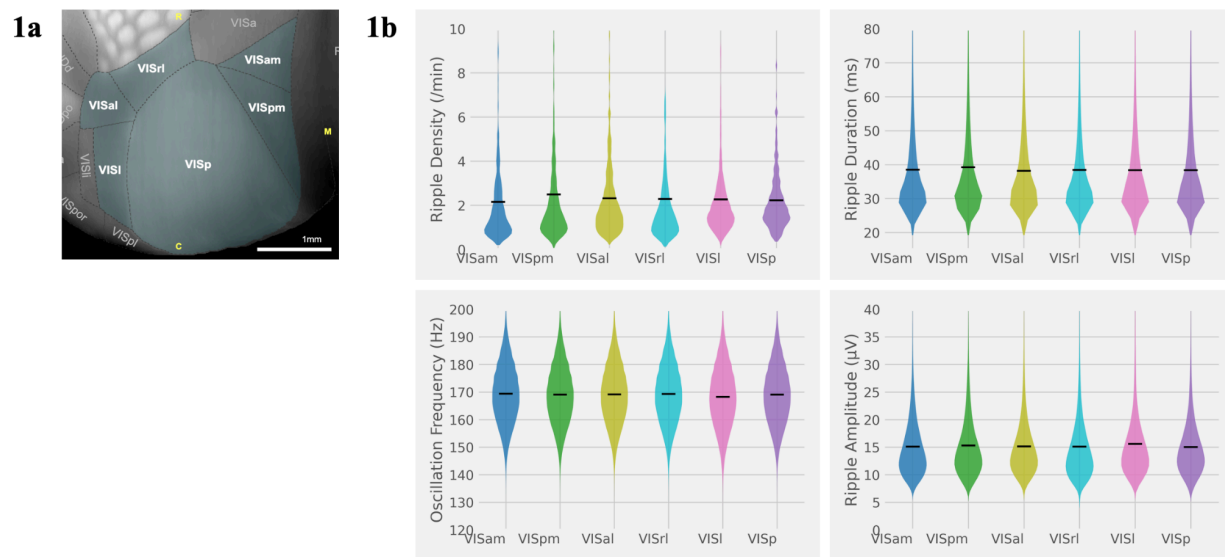


**Fig.1a** obtained from the Allen Institute

(<https://portal.brain-map.org/circuits-behavior/visual-behavior-neuropixels>), illustrates the spatial distribution of the six visual areas recorded. **Fig.1b** summarizes ripple properties averaged across 65 sessions and the full recording duration. Y-axis limits were arbitrarily set for readability.

We first examined the basic properties of ripples detected using CSD across the six visual cortical areas, aggregating data from all 65 analyzed sessions (Fig. 1b). Ripple density showed moderate variation, with VISpm exhibiting slightly higher rates. Most ripples were shorter than 40 milliseconds and had amplitudes below 15 microvolts. Oscillation frequency was consistent across areas, with a mean of around 170 Hz, which falls within the expected ripple range reported in previous studies for hippocampal ripples in rodents (Buzsáki et al., 2015; Liu et al., 2017; Oliva et al., 2018). The frequency distribution was approximately balanced between 140 Hz and 200 Hz. Overall, ripple characteristics were broadly similar across visual areas, with no pronounced differences.

## 2. Task- and stimulus-dependent modulation of cortical ripples



**Fig. 2a** shows the mean ripple count per 30-second bin across time for each visual area. The colored bar along the x-axis indicates stimulus blocks: active behavior, Gabors, spontaneous, full-field flashes, and passive replay. **Fig. 2b** shows the slope of ripple counts over time within each block, computed separately for active behavior and passive replay. Wilcoxon signed-rank tests with FDR correction were used to compare slope distributions between conditions for each area. **Fig. 2c** shows area-wise ripple slopes compared to the baseline area (VISam), using two-sided Mann–Whitney U tests with FDR correction across areas. Left: active behavior. Right: passive replay. **Fig. 2d** shows ripple counts by cortical layer and area, normalized by channel count. Left: active behavior. Right: passive replay. All plots are averaged across 65 sessions. Shaded areas indicate SEM. Statistical significance: \* $p < 0.05$ , \*\* $p < 0.01$ , \*\*\* $p < 0.001$ .

To examine how ripple activity varies with task context and stimulus presentation, we analyzed ripple counts across time and stimulus blocks (Fig. 2). Ripple occurrence showed clear transitions at task boundaries, with sharp changes in density corresponding to different stimulus conditions (Fig. 2a). Ripple rates were lowest during spontaneous blocks, where mice viewed a static gray screen, and increased substantially during visually driven blocks, particularly during Gabor presentations and natural image viewing.

Although the same set of natural images was presented, ripple dynamics differed between active behavior and passive replay blocks. To quantify how ripple activity changed over time within each block, we fitted a linear regression to the ripple trajectories over time for each visual area, separately for the active and passive blocks. The resulting slope values were then compared across conditions and areas (Fig. 2b, 2c). As shown in Fig. 2b, these slopes (indicating ripple trends) significantly differed between active and passive blocks for all areas except VISpm.

To test whether ripple trends also reflected the hierarchical organization of the visual cortex, we compared slope values across areas between the active and passive blocks. As shown in Fig. 2c (left), during active behavior, ripple slopes followed a pattern that could be broadly grouped by the visual hierarchy described by Siegle et al. (2021): higher-hierarchy areas such as VISam and VISpm showed mildly negative slopes, mid-hierarchy areas like VISal and VISrl showed mildly positive slopes, and lower-hierarchy areas such as VISl and VISp showed the strongest positive slopes. This structured pattern was absent in the passive replay block (Fig. 2c, right), where slopes across areas did not significantly differ from the baseline (VISam), except for VISal. Raw ripple counts further illustrated these differences (Fig. 2a). During active behavior, ripple counts were initially high in higher-order associative areas (VISam and VISpm) and declined over time. In passive viewing, ripple counts remained consistently higher in lower-order areas (VISp and VISl) across the entire block.

Lastly, ripple distribution across cortical layers also varied between active and passive blocks (Fig. 2d). In the active block, ripple counts increased from superficial layers to deep layers, peaking at layer 5, whereas in the passive one, ripple distribution across layers was flatter and less structured. Type III ANOVA confirmed significant effects of task condition, area, cortical layer, and their interactions on ripple counts.

### **3. Co-ripples exhibit task-specificity**

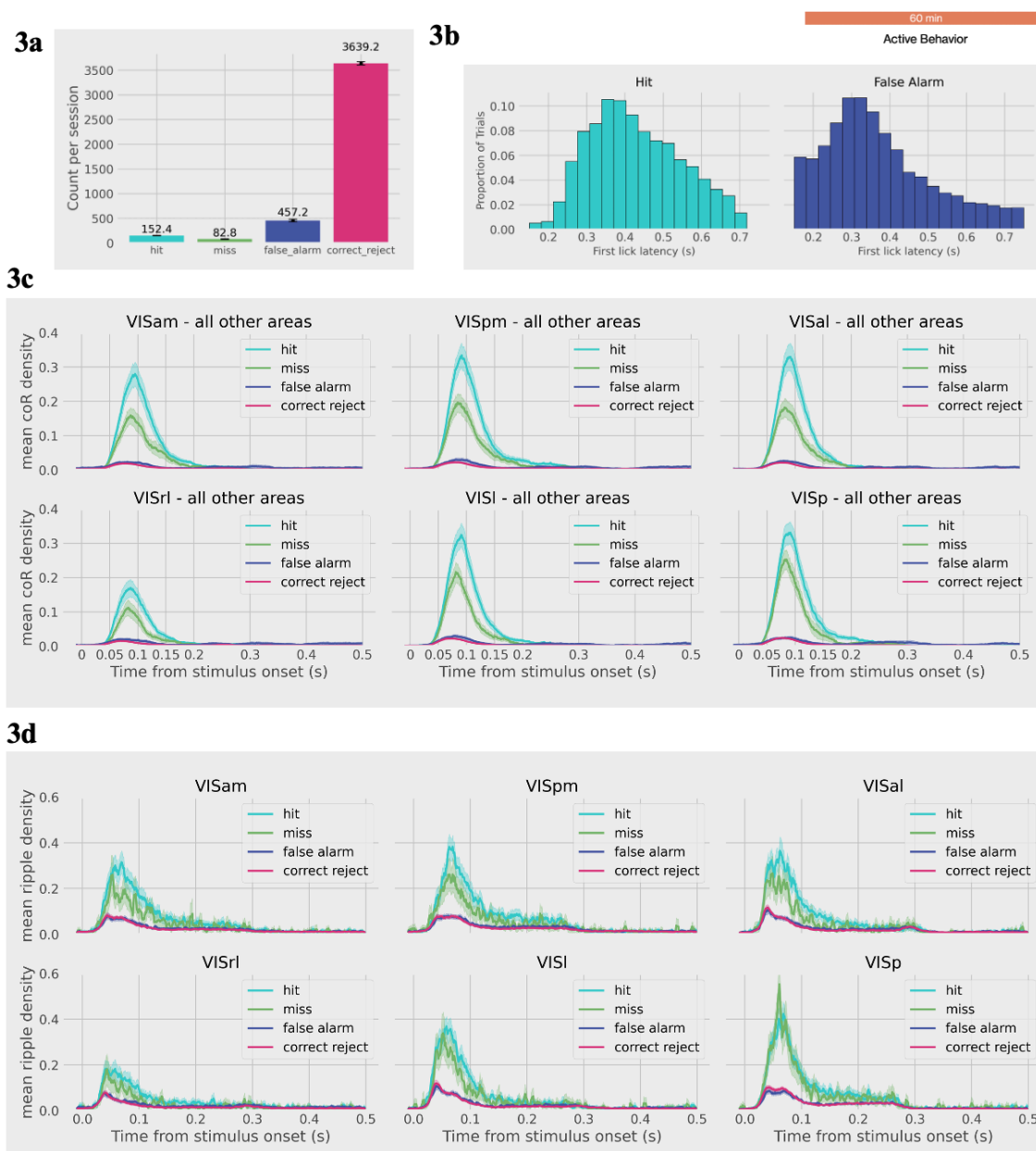


**Fig. 3a** shows the average number of trials per task condition across 65 sessions. Trials with premature licks (<150 ms after stimulus onset) were excluded. **Fig. 3b** displays normalized histograms of first lick latencies for hit (left) and false alarm (right) trials. **Fig. 3c** shows mean co-ripple density between each visual area and all other areas, grouped by task condition and aligned to stimulus onset. **Fig. 3d** shows mean ripple density for each visual area, grouped by task condition and aligned to stimulus onset. All plots are averaged across 65 sessions. Shaded areas indicate SEM.

Before analyzing co-ripples in relation to behavior, we examined trial structure and behavioral performance during the active behavior block across all sessions. Stimulus-change trials were

relatively infrequent compared to non-change trials, and correct rejects made up the majority of trials, indicating reliable suppression of responses when no change occurred (Fig. 3a). In hit trials, first lick latencies peaked around 0.35 seconds, while false alarm trials showed a similar peak with a greater proportion of early responses (Fig. 3b).

Co-ripple density varied significantly by task condition (Fig. 3c). Co-ripple density was highest during hit trials, where the mouse correctly detected a stimulus change, and this pattern was consistent across all visual areas. Co-ripple density in hit trials peaked between 99–125 ms after stimulus onset, exceeding pre-stimulus baseline by more than tenfold, and was on average twice as high as peaks in miss trials, where a change occurred but the mouse failed to respond. In contrast, false alarm and correct reject trials exhibited minimal co-rippling, remaining near baseline levels. Interestingly, the timing of co-ripple peaks varied by task. Peak latencies during hit trials were consistently later than during miss trials by 8–20 ms, depending on area. Similarly, false alarm trials showed later co-ripple peaks than correct rejects, with average delays of 23–33 ms. Though these later peaks in hits and false alarms appear associated with lick response, further statistical testing will be required to determine whether this shift reflects a functional difference.

To compare co-ripples with single-region ripple activity, we computed ripple density across all areas and task conditions (Fig. 3d). While ripple density increased during both hit and miss trials, the difference between the two was notably smaller than in co-ripples. In VISp, ripple traces for hit and miss trials were nearly indistinguishable. Ripple density was also more variable overall, but peak timing still followed the same pattern: hit trials peaked later than miss trials.

At present, we did not observe a clear relationship between either ripple or co-ripple activity and cortical hierarchy under these task conditions. Additional analyses will be conducted in the future to explore this possibility.

#### **4. Co-ripples exhibit layer-specificity during hit trials.**

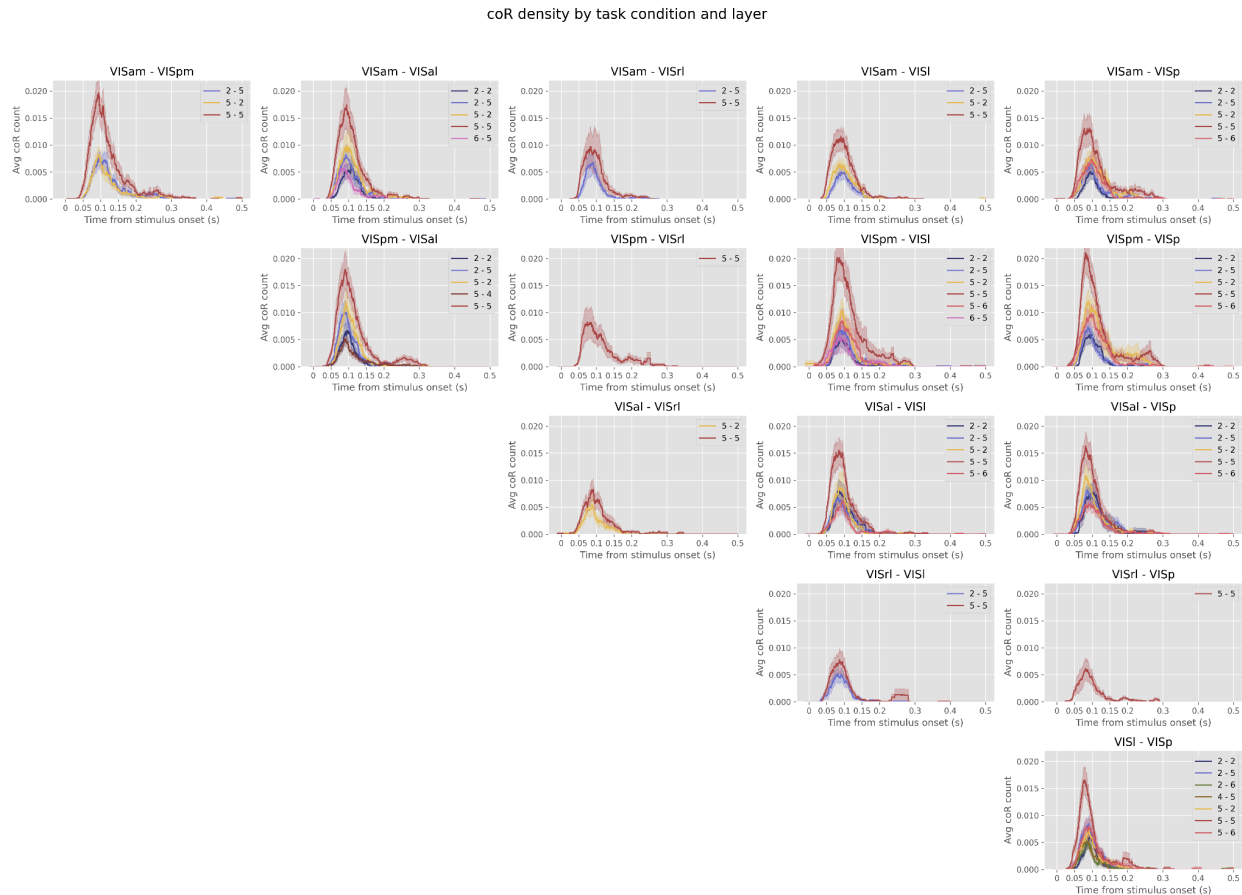


**Fig. 4** shows the mean co-ripple density for each possible visual area pair, grouped by task condition and further by cortical layer, aligned to stimulus onset. For readability, only layer-to-layer pairs with peak co-ripple density greater than 0.005 are shown. The legend follows the convention “first visual area layer X – second visual area layer Y.” Visual area pairs are ordered by cortical hierarchy from high to low, from left to right and top to bottom in the plot. The plot is averaged across 65 sessions. Shaded areas indicate SEM.

To further investigate the laminar organization of co-ripples, we broke down co-ripple density by cortical layer for each visual area pair and task condition (Fig. 4). Among all layer-to-layer combinations, deep–deep interactions (layer 5 to layer 5) consistently showed the highest peak co-ripple density across visual area pairs. This strong coupling may partly reflect the fact that layer 5 had the highest overall ripple counts across areas (Fig. 2d, left), so additional normalization will be done in the future to account for baseline ripple levels.

Cross-laminar pairs, specifically layer 2/3 to layer 5 and layer 5 to layer 2/3, showed the next highest co-ripple densities. When examined in the context of cortical hierarchy, co-ripple density was often higher for projections originating in lower-hierarchy area layer 5 and targeting higher-hierarchy area layer 2/3, compared to the reverse direction. This asymmetry was more

pronounced in lower-hierarchy area pairs than in higher-hierarchy ones. However, further quantification will be necessary to determine the significance and consistency of this directional difference.

## Discussion

In this study, we characterized locally generated cortical ripples from the mouse visual cortex using current source density (CSD), revealing consistent ripple properties across six visual cortical areas. The ripples showed distinct temporal patterns across different stimuli, with notable modulation by behavioral context. Even when identical stimuli were presented, ripple dynamics differed significantly depending on task engagements. Specifically, during the active change-detection block, ripples initially predominated in higher-order associative areas (VISam and VISpm) gradually declining, whereas ripple counts progressively increased in lower-order visual areas (VISp and VISl) and remained consistently elevated throughout the passive replay block. Together with observed laminar differences in ripple density between active and passive blocks, these findings indicate that ripple activity is not driven purely by sensory input alone but is strongly influenced by task engagements, and this influence is selectively expressed across cortical hierarchies and laminar organization.

A finding of our study is the robust task-specific modulation of co-ripples across all visual areas. Co-ripple density was particularly prominent in hit trials compared to other trial types, reinforcing the notion that co-ripples reflect more than mere sensory stimulation. They are closely linked to perceptual decisions and behavioral outcomes. The clear distinction between hit trials (true positives) and false alarm trials (false positives) in terms of co-ripple density parallels recent findings in the human cortex during a word-matching task (Garrett et al., 2024). This parallel suggests that task-dependent modulation of co-ripples is a conserved neural mechanism across species, tasks, and cortical regions.

Notably, the differences between task conditions were less distinct and clear in single-area ripple densities compared to co-ripples, suggesting that it's the cross-area co-ripples rather than the within-area ripples that play a critical role in cortical coordination. Such a pattern supports the central hypothesis that cortico-cortical ripples play a fundamental role in integration of cortical regions that facilitate information processing.

Our laminar analyses uncovered additional layer-specific insights into ripple organization. Deep cortical layers, especially layer 5 (the “output layer”), showed prominent ripple and co-ripple activities. Cross-laminar co-ripples, particularly between layers 2/3 and 5, suggest the presence

of specialized pathways facilitating interlaminar coordination. However, further normalization and statistical approaches are necessary to interpret those findings.

## **Future Directions**

Future analyses will expand upon our characterization of co-ripples, particularly their temporal and functional properties. We plan to investigate the phase relationships of co-ripples, including phase-locking and phase lags between visual areas, and to further clarify the observed laminar differences. We will also relate co-ripple dynamics to the visual cortical hierarchy. Additionally, we will compare co-ripple densities between active behavior and passive replay blocks to determine whether task engagement significantly modulates co-ripple patterns (an expected outcome if co-ripples indeed support task-dependent cortical integration).

Beyond characterizing co-ripples themselves, we also plan to explore their relationship with neuronal firing patterns. Very preliminary observations have indicated that ripples are positively correlated with multiunit activity (MUA) with a consistent temporal lag. Further analyses will quantify phase lags between ripples and MUA, and assess how co-ripples influence single-unit co-firing, building upon prior findings in humans suggesting co-ripples enhance unit co-firings (Verzhbinsky et al., 2023). Lastly, using optotagged Sst and Vip interneurons, we could clarify how different neuron types are selectively modulated by co-ripples, which could reveal cell-type-specific contributions to ripple-mediated cortical communication.

## References

- Allen Institute for Brain Science (2020). layer\_mapping.py [software script]  
[https://www.dropbox.com/scl/fo/6x7ovegu2jp4jxrhyv0fi/APGHNCbZrJFU6xfccmyu1Vw?dl=0&e=1&preview=layer\\_mapping\\_example.py&rlkey=qqn8efbm4pto0olh0g9o5ctjs](https://www.dropbox.com/scl/fo/6x7ovegu2jp4jxrhyv0fi/APGHNCbZrJFU6xfccmyu1Vw?dl=0&e=1&preview=layer_mapping_example.py&rlkey=qqn8efbm4pto0olh0g9o5ctjs)
- Allen Institute for Brain Science (2019). *Allen Brain Observatory - Neuropixels Visual Coding (Version 1.0, 10.1.19)*. Retrieved from <https://brain-map.org>
- Allen Institute. (2022). *Visual Behavior Neuropixels: Technical Whitepaper (Version 1.0, 8.16.22)*. Retrieved from <https://brain-map.org>
- Buzsáki, G. (2015). Hippocampal sharp wave-ripple: A cognitive biomarker for Episodic Memory and Planning. *Hippocampus*, 25(10), 1073–1188. <https://doi.org/10.1002/hipo.22488>
- Dickey, C. W., Verzhbinsky, I. A., Jiang, X., Rosen, B. Q., Kajfez, S., Eskandar, E. N., Gonzalez-Martinez, J., Cash, S. S., & Halgren, E. (2022). Cortical ripples during NREM sleep and waking in humans. *The Journal of Neuroscience*, 42(42), 7931–7946. <https://doi.org/10.1523/jneurosci.0742-22.2022>
- Dickey, C. W., Verzhbinsky, I. A., Jiang, X., Rosen, B. Q., Kajfez, S., Stedelin, B., Shih, J. J., Ben-Haim, S., Raslan, A. M., Eskandar, E. N., Gonzalez-Martinez, J., Cash, S. S., & Halgren, E. (2022). Widespread ripples synchronize human cortical activity during sleep, waking, and memory recall. *Proceedings of the National Academy of Sciences*, 119(28). <https://doi.org/10.1073/pnas.2107797119>
- Fabo, D., Bokodi, V., Szabó, J.-P., Tóth, E., Salami, P., Keller, C. J., Hajnal, B., Thesen, T., Devinsky, O., Doyle, W., Mehta, A., Madsen, J., Eskandar, E., Erőss, L., Ulbert, I., Halgren, E., & Cash, S. S. (2023). The role of superficial and deep layers in the generation of high frequency oscillations and interictal epileptiform discharges in the human cortex. *Scientific Reports*, 13(1). <https://doi.org/10.1038/s41598-022-22497-2>
- Fries, P. (2009). Neuronal gamma-band synchronization as a fundamental process in cortical computation. *Annual Review of Neuroscience*, 32(1), 209–224. <https://doi.org/10.1146/annurev.neuro.051508.135603>
- Garrett, J. C., Verzhbinsky, I. A., Kaestner, E., Carlson, C., Doyle, W. K., Devinsky, O., Thesen, T., & Halgren, E. (2024). Binding of cortical functional modules by synchronous high-frequency oscillations. *Nature Human Behaviour*, 8(10), 1988–2002. <https://doi.org/10.1038/s41562-024-01952-2>
- Gray, C. M., König, P., Engel, A. K., & Singer, W. (1989). Oscillatory responses in Cat Visual Cortex Exhibit inter-columnar synchronization which reflects global stimulus properties. *Nature*, 338(6213), 334–337. <https://doi.org/10.1038/338334a0>
- Hunter, J. D. (2007). Matplotlib: A 2D graphics environment. *Computing in Science & Engineering*, 9(3), 90–95. <https://doi.org/10.1109/mcse.2007.55>
- Jiang, X., Gonzalez-Martinez, J., & Halgren, E. (2019). Posterior hippocampal spindle ripples co-occur with neocortical theta bursts and downstates-upstates, and phase-lock with parietal spindles during NREM sleep in humans. *The Journal of Neuroscience*, 39(45), 8949–8968. <https://doi.org/10.1523/jneurosci.2858-18.2019>
- Khodagholy, D., Gelineas, J. N., & Buzsáki, G. (2017). Learning-enhanced coupling between ripple oscillations in association cortices and hippocampus. *Science (New York, N.Y.)*, 358(6361), 369–372. <https://doi.org/10.1126/science.aan6203>

- Liu, Y., McAfee, S. S., & Heck, D. H. (2017). Hippocampal sharp-wave ripples in awake mice are entrained by respiration. *Scientific Reports*, 7(1). <https://doi.org/10.1038/s41598-017-09511-8>
- Oliva, A., Fernández-Ruiz, A., Fermino de Oliveira, E., & Buzsáki, G. (2018). Origin of gamma frequency power during hippocampal sharp-wave ripples. *Cell Reports*, 25(7). <https://doi.org/10.1016/j.celrep.2018.10.066>
- Pedrosa, R., Nazari, M., Mohajerani, M. H., Knöpfel, T., Stella, F., & Battaglia, F. P. (2022). Hippocampal gamma and sharp wave/ripples mediate bidirectional interactions with cortical networks during sleep. *Proceedings of the National Academy of Sciences*, 119(44). <https://doi.org/10.1073/pnas.2204959119>
- Revonsuo, A., & Newman, J. (1999). Binding and consciousness. *Consciousness and Cognition*, 8(2), 123–127. <https://doi.org/10.1006/ccog.1999.0393>
- Seabold, S., & Perktold, J. (2010). Statsmodels: Econometric and statistical modeling with python. *Proceedings of the Python in Science Conference*, 92–96. <https://doi.org/10.25080/majora-92bf1922-011>
- Shadlen, M. N., & Movshon, J. A. (1999). Synchrony unbound: A critical evaluation of the temporal binding hypothesis. *Neuron*, 24(1), 67–77. [https://doi.org/10.1016/S0896-6273\(00\)80822-3](https://doi.org/10.1016/S0896-6273(00)80822-3)
- Siegle, J. H., Jia, X., Durand, S., Gale, S., Bennett, C., Graddis, N., Heller, G., Ramirez, T. K., Choi, H., Luviano, J. A., Groblewski, P. A., Ahmed, R., Arkhipov, A., Bernard, A., Billeh, Y. N., Brown, D., Buice, M. A., Cain, N., Caldejon, S., ... Koch, C. (2021). Survey of spiking in the mouse visual system reveals functional hierarchy. *Nature*, 592(7852), 86–92. <https://doi.org/10.1038/s41586-020-03171-x>
- Singer, W. (1994). The role of synchrony in neocortical processing and synaptic plasticity. *Physics of Neural Networks*, 141–173. [https://doi.org/10.1007/978-1-4612-4320-5\\_4](https://doi.org/10.1007/978-1-4612-4320-5_4)
- Singer, W. (2021). Recurrent dynamics in the cerebral cortex: Integration of sensory evidence with stored knowledge. *Proceedings of the National Academy of Sciences*, 118(33). <https://doi.org/10.1073/pnas.2101043118>
- Suh, J., Foster, D. J., Davoudi, H., Wilson, M. A., & Tonegawa, S. (2013). Impaired hippocampal ripple-associated replay in a mouse model of schizophrenia. *Neuron*, 80(2), 484–493. <https://doi.org/10.1016/j.neuron.2013.09.014>
- Vallat, R. (2018). Pingouin: Statistics in python. *Journal of Open Source Software*, 3(31), 1026. <https://doi.org/10.21105/joss.01026>
- Verzhbinsky, I. A., Rubin, D. B., Kajfez, S., Bu, Y., Kelemen, J. N., Kapitonava, A., Williams, Z. M., Hochberg, L. R., Cash, S. S., & Halgren, E. (2023). Co-occurring ripple oscillations facilitate neuronal interactions between cortical locations in humans. *Proceedings of the National Academy of Sciences*, 121(1). <https://doi.org/10.1073/pnas.2312204121>
- Vinck, M., Uran, C., Spyropoulos, G., Onorato, I., Broggin, A. C., Schneider, M., & Canales-Johnson, A. (2023). Principles of large-scale neural interactions. *Neuron*, 111(7), 987–1002. <https://doi.org/10.1016/j.neuron.2023.03.015>
- Virtanen, P., Gommers, R., Oliphant, T. E., Haberland, M., Reddy, T., Cournapeau, D., Burovski, E., Peterson, P., Weckesser, W., Bright, J., van der Walt, S. J., Brett, M., Wilson, J., Millman, K. J., Mayorov, N., Nelson, A. R., Jones, E., Kern, R., Larson, E., ... Vázquez-Baeza, Y. (2020). SciPy 1.0: Fundamental algorithms for scientific computing in python. *Nature Methods*, 17(3), 261–272. <https://doi.org/10.1038/s41592-019-0686-2>

- von der Malsburg, Ch., & Schneider, W. (1986). A neural cocktail-party processor. *Biological Cybernetics*, *54*(1), 29–40. <https://doi.org/10.1007/bf00337113>
- von der Malsburg, Christoph. (1994). The correlation theory of brain function. *Physics of Neural Networks*, 95–119. [https://doi.org/10.1007/978-1-4612-4320-5\\_2](https://doi.org/10.1007/978-1-4612-4320-5_2)
- Wang, Q., Ding, S.-L., Li, Y., Royall, J., Feng, D., Lesnar, P., Graddis, N., Naeemi, M., Facer, B., Ho, A., Dolbeare, T., Blanchard, B., Dee, N., Wakeman, W., Hirokawa, K. E., Szafer, A., Sunkin, S. M., Oh, S. W., Bernard, A., ... Ng, L. (2020). The Allen Mouse Brain Common Coordinate Framework: A 3D reference atlas. *Cell*, *181*(4). <https://doi.org/10.1016/j.cell.2020.04.007>